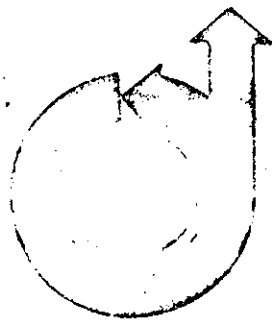

AIAA Paper
No. 72-70

(3)

INFRARED DETECTION OF HF TRACER GAS IN INERT AND COMBUSTING FLOWS

by
P. C. MALTE and J. A. NICHOLLS
The University of Michigan
Ann Arbor, Michigan

AIAA PAPER 72-70

AIAA 10th Aerospace Sciences Meeting
SAN DIEGO, CALIFORNIA/JANUARY 17-19, 1972

18

INFRARED DETECTION OF HF TRACER GAS IN INERT AND COMBUSTING FLOWS*

P. C. Malte** and J. A. Nicholls
Aerospace Engineering, The University of Michigan
Ann Arbor, Michigan

Abstract

A noninterferring diagnostic technique that employs monomeric hydrogen fluoride, HF, as a passive tracer gas has been developed. Infrared absorption by HF is used to infer turbulent mixing rates in inert and combusting flows. Data are presented on the turbulent diffusion of HF seeded streams of air, heated air, H_2, and CO_2 into an outer coaxial air stream. Combustion of C_2H_2 and air in a free jet configuration has also been investigated with the HF tracer. In most of these flow situations, the HF exhibited apparent rotational nonequilibrium. Development of the experimental technique and methods for data acquisition and analysis are discussed.

I. Introduction

Infrared absorption by trace amounts of HF offers a new and quantitative means of gaseous flow "visualization". The optical HF diagnostic technique is applicable to experimental research on turbulent mixing phenomena in both inert and combusting flows. For instance, turbulent mixing between two streams can be "mapped" without flow distortion due to physical probes. Likewise, turbulent diffusion in combustion flows, such as the primary zone of a gas turbine combustor liner, can be studied without the use of water cooled sampling probes.

The general experimental technique, as applied to cylindrically symmetric flows, is summarized below. Trace amounts (typically 3 molar per cent) of monomeric hydrogen fluoride, HF, are injected into a selected gas stream. Downstream, in a resulting, turbulently mixing flow, either inert or combusting, tracer concentrations are determined by spectroscopic observation of the R-branch of the fundamental vibration-rotation band of the HF spectrum. Transverse optical scans of the gas jet are made and path integrated absorptances at the peak of selected isolated HF spectral lines measured. The situation is illustrated in Fig. 1. These data are numerically Abel inverted and radial distributions of tracer concentrations are determined. The required computation technique employs a generalized extension of the Ladenburg-Reiche[1] curve-of-growth. The method is applicable to nonhomogeneous flows with foreign gas broadening of "weak" to "nearly-strong" spectral line absorptances.

Hydrogen fluoride has been chosen as the tracer gas for a number of reasons. It is a strong absorber in its fundamental vibration-rotation band centered at 2.5μ. The R-branch of this band, as shown in Fig. 2, extends into spectral regions devoid of interference by H_2O and CO_2, as well as most hydrocarbons and other combustion products[2], i.e., CO, NO, etc. Strong bonding between hydrogen and fluorine atoms allows its use at high temperature. The spectral line spacing is such that a single line may be easily isolated with monochromators of moderate resolution. Finally, spectral line strengths and half-widths of HF are fairly well known.

The chemical and thermodynamic properties of hydrogen fluoride make it somewhat less desirable to use as a tracer gas. To ensure tracer inertness, the following chemical characteristics of hydrogen fluoride must be considered and their effects minimized: its strong affinity for liquid water, adherence to and reaction with metal surfaces, and molecular polymerization of the gas at conditions near its saturated vapor state. Monomer thermodynamic non-ideality is additionally possible due to van der Waals forces[3]. Furthermore, the slow relaxation of gaseous HF to thermodynamic equilibrium with resultant rotational population distributions differing from Maxwell-Boltzman statistics is indicated as possible for the experimentation reported herein.

The detailed development of the HF diagnostic technique is given in Ref. 4, 5, 6, and 7. Latest methods concerning experimental technique and data acquisition and analysis are given in this presentation. Most recent data have been obtained to verify the preciseness of the HF technique.

---

*The research reported here constitutes, in part, the Ph.D. thesis of P. C. Malte who was supported by a NASA and an NSF traineeship. Support was also received from the university's Institute for Environmental Quality. Earlier work and much of the experimental apparatus were derived from contracted work with the Aero Propulsion Laboratory, Wright-Patterson Air Force Base, Ohio.

**Advanced Technology Staff, Rohr Corporation, Chula Vista, California.

Results are presented for non-burning free coaxial jet mixing experiments wherein HF seeded jets of air, heated air, H_2, and CO_2 mix with a uniform outer stream of air. For this flow configuration, both the centerline velocity and outer stream velocity are approximately 45 meters/sec. Conservation of HF mass flow in the jet systems is established and radial tracer concentration profiles are compared with known mixing layer and jet similarity profiles. The degree of thermodynamic nonequilibrium of the HF is discussed.

A flame experiment with an acetylene-air-HF mixture substituted for the inner jet, and still using the equal velocity outer air jet, was also conducted. The combustible mixture was spark ignited and the flame "stabilized" at the base of the inner jet tube wall. Measurements of the turbulent spread of the HF tracer, flame temperature distributions, and HF rotational thermodynamic state are discussed.

II. Optical Method

Configuration and Apparatus

The experimental configuration necessary for the optical absorption measurements is illustrated schematically in Fig. 1. The nonhomogeneous circular jet is seeded with spectrally active tracer gas. Radiant energy, I_ν^o, is directed from the light source, attenuated by the gas jet, and collected and measured at the monochromator. Absorption of radiant energy by the HF tracer at discrete wavelengths near 2.5μ (also expressible in wave numbers as 4000 cm^{-1}) is shown in Fig. 2*. The amount of absorption at the center of each isolated spectral line is related to the tracer concentration and its molecular state in the gas jet. In this case, it must be noted that effects are integrated along the nonhomogeneous active optical path delimited by the gas jet boundaries.

Major optical components, as shown in Fig. 3, include a tungsten light source, 100 hz chopper, f/12 mirror system, and grating monochromator (Perkin-Elmer Model 98G) with an uncooled lead sulfide photoconductivity cell detector (Kodak Ektron Type N). These optical components are mounted on a platform. Motorized movement of the platform facilitates jet scanning. The height of the optical platform relative to jet axial position is set manually. Signal measurement, with required electronic instrumentation, follows standard practices[8] and is illustrated in Fig. 4. The primary component is a lock-in-amplifier (PAR Model 120) for signal demodulation and amplification. A more detailed account of the optical set-up and instrumentation is given in Ref. 6.

Spectral line measurements of emission of radiant energy from hot gases are also obtained with this system. In this case the chopper is placed immediately preceding the monochromator entrance slit.

Mathematical Formulation

The radiative transfer equation is utilized to mathematically describe the above optical arrangement. The equation includes absorption and emission coefficients which are related to the molecular and thermodynamic properties of the gas. With reference to Fig. 1 and 3, the radiant energy, I_ν, emerging from the jet boundary nearest the observer (monochromator) is given by the radiative transfer equation[9,10] as:

$$I_\nu = I_\nu^o \exp\left(-\int_0^L Pk_\nu \, d\ell\right) + \int_0^L Pk_\nu \, B_\nu \exp\left(-\int_0^\ell Pk_\nu \, d\xi \; d\ell\right) \qquad (1)$$

The gas is assumed to be in local thermodynamic equilibrium with emission and absorption coefficients related by Kirchhoff's law[9,10]. In Eq. (1), the term P is the partial pressure of the spectrally active gas, ν is the radiation frequency in wave numbers, k_ν is the absorption coefficient, B_ν is the Planck black body function, and ℓ is the distance along the optical path of total length L.

The second term on the right-hand side of Eq. (1) represents the spontaneous emission of radiant energy, $I_{\nu e}$, while the loss of radiant energy of the incident light beam is expressed by the absorption.

$$a_\nu = 1 - \frac{I_\nu - I_{\nu e}}{I_\nu^o} = 1 - \exp\left(-\int_0^L Pk_\nu \, d\ell\right) \qquad (2)$$

For gases at low temperature, the Planck black body function is small and consequently $I_{\nu e}$ exhibits a negligible value. At increased temperatures, one must measure both I_ν (light source on) and $I_{\nu e}$ (light source extinguished) in order to determine the true absorption, a_ν.

*For spectral line R(J), the HF molecule, upon absorption of radiant energy, undergoes a transition from molecular vibrational ground state (v = 0) to the first vibrational level (v = 1). Simultaneously, the molecular rotation changes from state J to J + 1.

$$y_L \to \infty \; ; \; W \to 2\left(\int_0^L PSb\, d\ell\right)^{1/2} \; ; \; F \to \frac{b}{b_e} \qquad (12)$$

The limiting expressions for F are obtained since the limiting values of the equivalent width, for non-homogeneous media, can also be obtained using the standard unmodified Lorentz contour, Eq. (6). Furthermore, for values of y_L between 0 and 5 (weak through intermediate strength absorptances) the Ladenburg-Reiche curve-of-growth can be closely approximated by the following expression:

$$W = 2\pi\, b_e\, y_L \frac{1 + 0.0701\, y_L}{1 + 0.5884\, y_L} \; ;$$

$$0 \leq y_L \lesssim 5 \qquad (13)$$

Comparison of Eq. (9), (11), (12), and (13) is illustrated in Fig. 5.

Experimental Procedure and Analysis

As indicated above, the experimental technique relies on the measurement of the transverse distribution of $\bar{a}_{\nu c}$. During experimentation, the optical platform is positioned at the desired jet axial location, and the monochromator signal is "peaked" at the selected spectral line center. A transverse scan of the peak absorptance is then obtained by motorized optical platform movement, as illustrated by Fig. 1. Usually absorption scans for several different R-branch HF spectral lines are measured at each axial jet location. As will be shown, this is required for the determination of the molecular state of the tracer; necessary information for the calculation of tracer concentration from absorption measurements.

Data analysis of the transverse distributions of $\bar{a}_{\nu c}$ is initiated by digitizing recorded transverse profiles. Typically, the half profile of $\bar{a}_{\nu c}$ is divided into 20 zones. Zonal values are labeled $\bar{a}_n$. Corresponding values of equivalent width are determined via Eq. (5). The slit width $\Delta\nu$, which is a function of frequency, $\bar{\nu}$, is determined by previous monochromator calibration. With initial estimates for b_{en}, via Eq. (7), using temperature and partial pressure estimates, Eq. (12) is solved to obtain the transverse distribution, y_{Ln}. Abel inversion of the y_{Ln} distribution yields the radial digital distribution of the integral of Eq. (9), i.e. $(PS)_k$.

With b_{en} values evaluated at the center of each optical path, L_n, the following "universal" relation is valid:

$$F = 1 \qquad (14)$$

Knowledge of the HF molecular state and the gas kinetic temperature, together with $(PS)_k$ values, yields a determination of tracer partial pressure radial distribution. Equation (7) is then used to re-evaluate b_{en} values, followed by a first iteration of the above computation technique. Convergence to 0.1% accuracy usually occurs in 3 to 4 iterations for non-burning flows. For spectral lines of weak and intermediate strengths uncertainties in spectral line half-widths, the conditional validity of Eq. (8), plus the effect of HF thermodynamic non-equilibrium exert a negligible to small effect on the calculated values of $(PS)_k$.

For HF at kinetic temperatures less than approximately 2000°K, the quantity PS depends solely on the number density of the lower quantum state (N_ℓ) corresponding to the observed radiative transition. The relation is

$$PS = \frac{\pi e^2}{mc^2} N_\ell\, f_{\ell u} \qquad (15)$$

The quantity $\pi e^2/mc^2$ has a constant value of 8.83×10^{-13} cm for HF, while $f_{\ell u}$ is the absorption oscillator strength. The parameter $f_{\ell u}$ possesses a different constant value for each spectral line; values for HF R-branch spectral lines are given in Ref. 15.

In practice the total tracer number density, N, at a selected position can be closely determined by summing corresponding N_ℓ values for all observable spectral lines in the R-branch of the fundamental band. However, for the investigations reported herein the HF tracer usually exhibited rotational population distributions according to "rotational" temperature T_J. With knowledge of rotational temperature T_J, the Maxwell-Boltzmann[10] population distribution can be used to obtain a measurement of total number density for the condition that all molecules exist in the ground vibrational state (implies that $T \lesssim 2000$°K for HF). The relation is given as follows:

$$\frac{N_\ell}{N} = \frac{N_J}{N} = \frac{(2J+1)\exp(-E_J/k\,T_J)}{\sum_{J=0}^{\infty}(2J+1)\exp(-E_J/k\,T_J)} \qquad (16)$$

where E_J is the quantized rotational energy of state J and k is the Boltzmann constant. As shown in Ref. 4, Eq. (15) and (16) can then be combined so that

$$N = \frac{(PS)}{(TS)} \frac{k}{1.013 \times 10^6} \qquad (17)$$

The parameter TS is only a function of rotational temperature and rotational quantum number J.

The rotational temperature is determined by plotting $\ln[N_\ell/2J+1]$ versus $J(J+1)$ from data obtained for at least two spectral line measurements. The straight line slope is calculated via the following equation:

$$\frac{d \ln[N_\ell/2J+1]}{dJ(J+1)} = \frac{-hc B_o}{kT_J} \quad (18)$$

Equation (18) is derived using Eq. (15) and (16) with the definition

$$E_J = hc B_o J(J+1) \quad (19)$$

where B_o is the rotational constant of the molecule, h is the Planck constant, and c is the speed of light. For complete thermodynamic equilibrium T_J equals the kinetic temperature T, a condition that was rarely satisfied for the reported experiments.

III. Tracer Preparation and the Flow System

In the current experimentation careful prepared samples of gaseous hydrogen fluoride monomer, HF, are obtained by heating quantities of polymerized liquid-vapor until complete vaporization and polymer "cracking" occur and the gaseous monomer state is confirmed. At moderate temperatures and pressures, gaseous hydrogen fluoride can exist as a combination[3] of the monomer, HF; dimer, H_2F_2; tetramer, H_4F_4; and hexamer, H_6F_6. The hexamer is the dominant polymer species. In Fig. 6, pressure P is plotted versus apparent association Z' for several temperatures of gaseous hydrogen fluoride. The apparent association is defined so that

$$P = \frac{\rho R_o T}{m_{HF} Z'} \quad (20)$$

where ρ is the gas density, R_o the universal gas constant, and m_{HF} the monomer molecular weight. To a small degree, the factor Z' also includes the effect of van der Waals forces for each molecular form of gaseous hydrogen fluoride.

Commercially available hydrogen fluoride is obtained in steel cylinders. Controlled heating of a cylinder in an oil bath to a temperature of approximately 50°C yields a vapor pressure of about 2 atmospheres. This vapor is allowed to flow into an evacuated copper cylinder. The cylinder is then heated, thereby vaporizing and "cracking" a controlled quantity of hydrogen fluoride. Prepared monomer samples usually exhibited a gas pressure of about 6 atm at 125°C for the experimentation reported herein. The monomer state is confirmed by observing perfect gas behavior of the pressure-temperature history during the latter stages of heating.

Once the sample is prepared, tracer measurements can be performed. With the current system, tracer flow rate is maintained constant with a corrosive gas regulator (Matheson Model B15-330) constructed with nickel coating, Monel metal, and a Kel-F diaphragm. Flow rate is monitored with a Teflon-Kel F rotometer manufactured by Mace Corporation (Model 900). Tubing and valves are constructed of Monel metal and Teflon to further limit system corrosion. Corrosion is additionally reduced by keeping the system dry. With this system, negligible corrosion was observed for 200 hours of exposure to pure hydrogen fluoride. Also, the delivery flow line, including regulator and rotometer is heated to a temperature controlled at approximately 100°C to prevent polymerization.

A schematic of the developed experimental flow system for HF preparation and delivery is shown in Fig. 7. Mixing of the HF with the selected test gas (air, CO_2, H_2, or C_2H_2 in these experiments) is accomplished at a venturi section. Mixing is completed in a "well-stirred" tank. For the current experiments, the mean residence time of gas in the "well-stirred" tank is about 1 second; furthermore, 95% of the gas molecules remained in the tank for time durations greater than 0.3 seconds. Mixing in the tank is accomplished by using several small nearly-sonic orifices.

The coaxial jet system is shown in Fig. 8. The jet nozzle exit is located 15 cm downstream of the "well-stirred" tank exit. With the configuration illustrated in Fig. 8, considerable turbulence is available from the wake formed at the base of the inner jet tube wall and from the center jet stream issuing from the "well-stirred" tank. The diameter of the outer air jet is 2.93 cm, while the inner jet i.d. is 0.746 cm with a 0.38 mm wall thickness. For flame measurements, the wall thickness is increased to 0.67 mm for a tube i.d. of 0.635 cm. In all experiments, both the centerline and uniform outer stream velocities are approximately 45 meters/second.

Besides the tracer absorption measurements, distributions of kinetic temperature, using thermocouples, and axial velocity, using impact probes are also measured in the jet flows. Dry nitrogen is substituted for the HF flow during impact probe measurements. In combusting flows, thermocouple measurements are corrected for radiation losses and velocity is measured in corresponding cold jet flows with equal flow rates and initial conditions.

IV. Experimental Results—Nonburning Mixing Layer Studies

First experiments were conducted with inner

jets of air seeded with HF and mixing turbulently with the outer coaxial stream. Data was obtained at several axial jet locations. Figure 9 presents results that show (within experimental error) similar mixing layer behavior following by a jet transition region. Nondimensional axial and radial distances are denoted by z/r_o and r/r_o, respectively. Mass concentration is denoted by κ and all initial (exit) jet conditions show a subscript "o". Beyond $z/r_o = 16$ the uniform character of the outer stream ceased due to mixing with its quiescent environment; the resultant mixing situation was more complicated than useful for these "check-out" experiments and therefore was not analyzed.

For this data, radial profiles of tracer concentration, velocity, and kinetic and HF rotational temperature are shown in Fig. 10. Data at the "near" station exhibit the following characteristics:

1. HF concentration—a uniform center core followed by a typical mixing layer spread.
2. Velocity—a nonuniform inner jet velocity profile along with a velocity deficit region near the tube wall base.
3. HF rotational temperature, T_J, not equal to the kinetic temperature, T, except near the outer region of HF spread.

At the "far" position, the tracer concentration exhibits a nearly-fully developed turbulent jet profile, while the gas velocity is nearly constant at 42 meters/second across the spectroscopically examined flow region. Some trend towards rotational relaxation of the HF to the local kinetic temperature is indicated at this position.

Constancy of tracer mass flow with increasing axial distance was observed in the jet system, thus indicating tracer chemical inertness. However, for the current experimental system these values were always about 40% less than the HF mass flow measurements obtained with both the rotometer and calculated from the nearly isothermal "cracker" (copper cylinder used for HF preparation) blowdown. This indicates a loss of HF tracer in the internal flow system via adherence to metal surfaces or chemical reactions at these surfaces.

Similar experiments with different inner jet gases and temperatures were conducted. Results are shown in Fig. 11, 12, and 13 for heated air, H_2, and CO_2, respectively. For the heated air and cold H_2 inner jet cases sufficiently rapid mixing occurred to establish a fully developed turbulent inner jet in the length allotted for uniform outer stream flow. As expected, most rapid mixing layer spread occurred with the H_2 jet.

The above experimental results have been compared with the classical turbulent mixing layer similarity solutions of Tollmien[18] and Görtler[19]. Tollmien and Görtler mixing layer solutions are derived for incompressible planar flows; furthermore, the Tollmien solution is strictly valid only whenever the outer stream has zero velocity, i.e. initial portion of a submerged jet. However, as verified in Ref. 20 and 21, these solutions are empirically valid for general incompressible mixing layers. Furthermore, the Taylor[22] vorticity analogy is utilized[20] to extend these solutions for velocity distribution to the case of admixture (tracer concentration) spread.

Agreement between the present experiments and the classical solutions is shown in Fig. 14. The turbulent similarity parameter, ϕ, defined for velocity, is zero at the half-velocity point, i.e. $u - u_e/u_{\mathfrak{C}_L} - u_e = 0.5$. The subscripts $\mathfrak{C}_L$ and e denote, respectively, the inner edge of mixing layer (jet $\mathfrak{C}_L$ value) and the outer edge. Present experiments yield a measurement of concentration rather than velocity spread; the corresponding radius at the "half-concentration" point is r_h, and accordingly, ϕ obtains the algebraic form shown in Fig. 14. The turbulent spread parameter, σ, is determined by matching the measured concentration profile with the classical solutions in the vicinity of the mid-point, i.e.

$$\sigma = (z + z_o) \frac{\partial(\kappa/\kappa_{\mathfrak{C}_L})/\partial r}{d(\kappa/\kappa_{\mathfrak{C}_L})/d\phi} \qquad (21)$$

The virtual origin of the mixing layer is denoted by z_o. At $\kappa/\kappa_{\mathfrak{C}_L} = 0.5$, the classical solutions yield[20] a slope $d(\kappa/\kappa_{\mathfrak{C}_L})/d\phi = 0.40$.

The spread of excess temperature is also shown for the heated air experiment. Since Taylor's[22] vorticity analogy predicts equivalence of the turbulent spread of heat and mass (temperature and admixture concentration) one would expect equal values for corresponding σ's and z_o's. The differences result since the initial temperature profile at the jet exit was nonuniform due to wall cooling effects while the tracer concentration profile was very nearly uniform across the inner jet exit.

For the mixing layer measurements summarized in Fig. 14, the relatively low σ values indicate rapid mixing which results from the high initial turbulent levels in the flow system. Since these measurements have been conducted to investigate the preciseness of the HF tracer technique, the following favorable results are summarized:

The HF tracer is chemically inert in the free flow systems.

nonideal and pressure dependent thermodynamic relaxation. Figure 17 indicates that for pressures below 0.01 atmospheres, thermodynamic equilibrium is nearly complete.

Initial Investigation of a Hydrocarbon Flame with HF Tracer

An acetylene-air flame, exhibiting an initial velocity field equivalent to that of the nonburning coaxial mixing experiments, has been examined using HF spectroscopy. The inner jet, consisting of a pre-mixed fuel-air composition with an equivalence ratio of 2.8, was again seeded with the HF tracer. The resultant spark ignition flame is shown in the schlieren photograph of Fig. 18.

Only radiation resulting from the HF tracer has been measured. The examined region, delimited by the schlieren photograph, exhibited "premixed" combustion; the wide annular outer or diffusion flame region emitted characteristic blue and violet radiation[25], with some turbulent fluctuations noted at its outer boundaries. Significant amounts of C_2H_2 in the central portion of the jet system remained unburned until the "downstream" portion of the flame was approached. The beginning of this region, which also coincides with the cessation of the uniform velocity field of the outer stream, is noted in the top areas of Fig. 18. Burning in the "downstream" region was rich in luminous carbon particles and exhibited a very turbulent and widespread diffusion-type[25] burning zone. Further examination of the schlieren photograph shows a well defined flame front in the "near-in" flow region with visible, nearly vertical, extension to a height of approximately $z/r_o = 15$.

Upon introduction of trace amounts of HF no significant change in flame shape or visible emitted radiation was noted. Furthermore, flow temperature measurements using a thermocouple yielded equivalent temperature field measurements (within experimental error) with and without the HF present. Thus, the combustion inhibition tendencies of halogen compounds, referred to briefly in Ref. 25, appear to be unimportant in the present situation employing trace amounts of HF.

A typical transverse scan of HF line absorption and emission is shown in Fig. 19. The profiles indicate a relatively cold jet centerline followed by low absorption levels in the flame and outer flame regions. The measured absorptances were Abel inverted with spectral line half-widths determined, in part, from the thermocouple measurements of kinetic temperature. Radial mapping of tracer concentration and kinetic temperature is shown in Fig. 20. Distributions of tracer concentration were determined from PS profiles and knowledge of kinetic and HF rotational temperatures. Rotational temperature was again determined by comparing several different spectral lines.

Examination of Fig. 20 shows a nearly similar mixing layer and indicates moderate mixing in the mid-regions of individual radial profiles followed by intensified spread, at low concentrations, in the outer flame region. This effect is especially noticeable for $z/r_o > 10.0$. In the flame front or peak temperature region, the nondimensional tracer concentration is typically 0.2 to 0.3. For the mixing layer the following values are determined for tracer concentration spread: $z_o/r_o = 6.3$ and $\sigma = 62.0$. Furthermore, the experimental mixing layer similarity profile, neglecting the extreme outer flame region, is in excellent agreement with the classical solutions of Fig. 14.

Comparison of the burning results with the above measurements of tracer concentration profiles in nonburning coaxial flows is interesting. With $\sigma = 62.0$ the combusting jet mixing layer exhibits the least spread. However, the result is somewhat misleading, since the combusting case also exhibits the greatest turbulent spread of the outer boundary of the HF seeded inner jet.

Again, the HF mass flow rate was found to be nearly constant in the jet system. As previously stated, velocities were measured in an equal flow rate inert system. About a 40% loss in HF flow rate in the internal flow system was again observed.

Measurements of kinetic and rotational temperatures are shown in Fig. 21 and 22 for $z/r_o = 2.56$ and 17.43, respectively. For the "near" position, $z/r_o = 2.56$, attempts to determine flame kinetic temperature based on emission-absorption pyrometry[9] were fairly successful. The computation technique, similar to the methods described in Ref. 25, included the significant effect of self-absorption of the emitted radiation. A slightly higher value for the peak flame temperature is determined with the pyrometric measurements, i.e. 1600°K versus 1400°K with the thermocouple scan. This difference, in part, results from calibration errors for the present optical system.

The HF rotational temperature was determined using the R(1), R(3), and R(4) spectral lines. Excellent straight line fits to plots of N_ℓ versus J, i.e. following the same procedure portrayed in Fig. 16, were obtained from the jet centerline to $r/r_o = 1.1$. Thereafter, due to the low values of N_ℓ and possible non-Maxwell-Boltzmann populations in the flame region only the R(4)/R(3) ratio yielded acceptable [illegible]

of rotational temperature. The measurements indicated a relaxation of HF towards the flame temperature conditions in the recirculation zone situated at the base of the inner jet tube wall. Again, the centerline HF rotational temperature is near 400°K; followed by some relaxation towards the colder center region temperature in the jet flow.

At increasing downstream axial positions thermocouple measurements were relied on completely to determine T. Due to emission profile asymmetry (see Fig. 19) and the influence of turbulent temperature fluctuations on measured emission, measurements of kinetic temperature by emission-absorption were increasingly unsatisfactory. Temperature measurements at the "far" position, $z/r_o = 17.43$, are shown in Fig. 22. While the centerline kinetic temperature increased to approximately 800°K, the HF rotational temperature appears to remain at approximately 400°K in the central region of the jet. Rotational temperature measurements using the three HF lines R(1), R(3), and R(4) were in agreement from centerline to $r/r_o = 2.0$; however, only trends at increased radial distances are indicated. Furthermore, the indicated increase in HF rotational temperature in the outer-flame region is believed to result, in part, from the streaming of rotationally excited molecules from the upstream recirculation zone.

Uncertainties in HF rotational state and temperature, as shown in Fig. 21 and 22 for $r/r_o > 1.1$ and 2.0, respectively, did have an unfavorable effect on number density determinations in these regions. The problem was lessened somewhat by using the spectral line with the least T_J dependence for number density determination, i.e. R(4). Also, only small tracer number densities were observed in the regions of T_J uncertainty, and therefore, the absolute effect on tracer radial distributions was small. Nevertheless a 50% error in concentration measurement is estimated for the regions of T_J uncertainty.

V. Conclusions

This study was undertaken to develop and evaluate HF tracer molecule diagnostics for application to turbulently mixing and reacting flows. For cold, radiatively absorbing flows the tracer technique appears to be precise and very useful. Most likely, the ultimate utility of the HF diagnostic technique is for turbulent mixing studies in reactive flows. In such situations the molecular state of the HF tracer is uncertain. Therefore, a detailed spectroscopic examination, using many of the observable R-branch spectral lines, is necessary. While these measurements would be tedious, their experimental potential cannot be overlooked. In combusting flows the tracer technique yields turbulent mixing rate data and response to changes in macroscopic flow properties; local concentrations of fuel, oxidizer, and product gases and their detailed thermodynamic states are not measured.

References

1. Ladenburg, R. and Reiche, F., "Uber Selektive Absorption," Am. Physik, Vol. 42, 1913, p. 181.

2. Pierson, R.H., Fletcher, A.N., and Gantz, E.S., "Catalog of Infrared Spectra for Qualitative Analysis of Gases," Analytical Chemistry, Vol. 28, 1956, p. 1218.

3. Smith, D.F., "Hydrogen Fluoride Polymer Spectrum, Hexamer and Tetramer," J.O.S.A., Vol. 28, 1958, p. 1040.

4. Malte, P.C., "Spectroscopic Detection of Hydrogen Fluoride Tracer in Gaseous Flow Systems," Ph.D. Thesis, The University of Michigan, 1971.

5. LaPointe, C.W. and Nicholls, J.A., "Supersonic Mixing and Combustion," Air Force Aero Propulsion Laboratory, Report TR-68-12, Wright Patterson Air Force Base, Ohio, 1968.

6. LaPointe, C.W., "An Optical Study of Coaxial Turbulent Mixing of Liquid and Gaseous Fuel with Air," Ph.D. Thesis, The University of Michigan, 1969.

7. LaPointe, C.W. and Malte, P.C., "Tracer Molecule Spectroscopy Applied to Turbulent Reactive Flows," AIAA Paper No. 70-726, San Diego, Calif., 1970.

8. Doebelin, E.O., Measurement Systems Application and Design, McGraw-Hill Book Co., New York, 1966.

9. Simmons, F.S., "Spectroscopic Pyrometry of Gases, Flames, and Plasmas," ISA Transactions, Vol. 2, 1963, p. 168.

10. Vincenti, W.G. and Kruger, C.H., Introduction to Physical Gas Dynamics, John Wiley and Sons, Inc., New York, 1965.

11. Dennison, D.M., "The Shape and Intensities of Infra-Red Absorption Lines," Physical Review, Vol. 31, 1928, p. 503.

12. Penner, S.S., Quantitative Molecular Spectroscopy and Gas Emissivities, Addison Wesley Publ. Co., Inc., Reading, Mass., 1959.

13. Smith, D. F., "Infrared Spectra Analysis for Hydrogen Fluoride," Spectrochemica Acta, Vol. 12, 1958, p. 224.

14. Simmons, F. S., "Radiances and Equivalent Widths of Lorentz Lines for Nonisothermal Paths," J. Q. R. S. T., Vol. 7. 1967. p. 111.

15. Meredith, R. E. and Kent, N. F., "Line Strength Calculations for the 0 - 1, 0 - 2, 0 - 3, and 1-2 Vibration-Rotation Bands of Hydrogen Fluoride," Willow Run Laboratories, Report 4613-125-T, The University of Michigan, 1966.

16. Jarry, R. L. and Daves, W., Jr., "The Vapor Pressure Association, and Heat of Vaporization of Hydrogen Fluoride," J. Am. Chem. Soc., Vol. 57, 1953, p. 600.

17. Long, R. W., Hildebrand, J. H., and Morrell, W. E., "The Polymerization of Gaseous Hydrogen and Deuterium Fluorides," J. Am. Chem. Soc., Vol. 65, 1943, p. 182.

18. Tollmien, W., "Berecknung Turbulenter Austreitungsvorgange," ZAMM, Vol. 6, 1926, p. 1. (Also, NACA TM 1085, 1945.)

19. Görtler, H., "Berechnung von Aufgaben der freien Turbulunz auf Grund eines neven Nakerungsansatzes," ZAMM, Vol. 22, 1942, p. 244.

20. Abramovich, G. N., The Theory of Turbulent Jets, M. I. T. Press, Cambridge, Mass, 1963.

21. Cohen, L. S., "A New Kinematic Eddy Viscosity Model," United Aircraft Research Laboratories Report G211709-1, East Hartford, Conn., 1968.

22. Taylor, G. I., "The Transport of Vorticity and Heat Transfer Through Fluids in Turbulent Motion," Proc. Roy. Soc., London, Vol. 135A, 1932, p. 685.

23. Smith, D. F., "The Overlapping Hydrogen Fluoride Monomer Dimer Spectra," J. Molecular Spec., Vol. 3, 1959, p. 473.

24. Lovell, R. J. and Herget, W. F., "Lorentz Parameters and Vibration-Rotation Interaction Constants for the Fundamental Band of HF," J. O. S. A., Vol. 52, 1962, p. 1374.

25. Gaydon, A. G., The Spectroscopy of Flames, John Wiley and Sons, Inc., New York, 1957.

26. Oss, J. P., "Absorption and Emission Coefficient Determination by a Zonal Ring Technique in a Circular Plasma Column," Aerospace Research Laboratories Report ARL 66-0110, Wright Patterson Air Force Base, Ohio, 1966.

Due to finite monochromator resolution, most isolated infrared spectral lines cannot be measured without some degree of distortion. With the recording monochromator centered at frequency $\bar{\nu}$, the measured (or apparent) absorption is expressed as:

$$\bar{a}_\nu = \frac{1}{\Delta\nu} \int_{slit} g(\nu - \bar{\nu})\, a_\nu \, d\nu \qquad (3)$$

The monochromator slit function is $g(\nu - \bar{\nu})$. By definition $g(0)$ is unity and the integral of $g(\nu - \bar{\nu})$ over ν is equal to the slit width $\Delta\nu$ (width of slit function at half-height).

Frequently, the monochromator slit function can be assumed triangular[11]. However, a simpler approximation assumes that the spectral line true absorption profile appears as a Dirac delta function to the slit function. Accordingly, one obtains

$$\bar{a}_\nu = \frac{1}{\Delta\nu} \int_{\bar{\nu}-\infty}^{\bar{\nu}+\infty} a_\nu \, d\nu \qquad (4)$$

Equation (4) is sufficient for present purposes; that is, the apparent absorption, as measured at frequency $\bar{\nu}$, is the average of the true absorption integrated over the slit width. The integral in Eq. (4) represents the equivalent width, W, of a spectral line; that is

$$W = \int_{\bar{\nu}-\infty}^{\bar{\nu}+\infty} a_\nu \, d\nu = \bar{a}_{\nu c}\, \Delta\nu \qquad (5)$$

The extra subscript "c" denotes the "centering" of the monochromator on a "narrow" spectral line satisfying the condition imposed by Eq. (4).

Evaluation of the integral in Eq. (5) yields the curve-of-growth for an isolated spectral line. The evaluation involves the use of Eq. (2), which in turn necessitates a formulation for the absorption coefficient k_ν. Spectral lines in the infrared are usually broadened by collisional processes[9]; the resultant profile for the absorption coefficient is described by the Lorentz contour[12]

$$k_\nu = \frac{S}{\pi b} \frac{1}{1 + \left(\frac{\nu - \bar{\nu}}{b}\right)^2} \qquad (6)$$

The spectral line strength is S, while the line half-width at half-height is b. Summing the collisional effects of all perturbers yields the following expression for line half-width:

$$b = \gamma \sum_s \alpha_s P_s \qquad (7)$$

The subscript "s" denotes species type, while α denotes the species broadening effectiveness relative to self-broadening. Various α-values for HF broadened by selected gases are given in Ref. 13. These values possess a weak temperature dependence at moderate temperatures. Also, for a given spectral line, the parameters S and γ are only temperature dependent; the temperature dependencies are plotted in Ref. 4 and 6.

Substitution of Eq. (6) into Eq. (2), followed by integration of Eq. (5) yields the well-known Ladenburg-Reiche[1] curve-of-growth if the gaseous medium is homogeneous. As shown by Simmons[14], it is possible to extend the Ladenburg-Reiche curve-of-growth to the case of non-homogeneous media. A modified Lorentz contour for the absorption coefficient, k_ν, of collision broadened spectral lines is utilized

$$k_\nu = \frac{SF}{\pi b_e} \frac{1}{1 + \left(\frac{\nu - \bar{\nu}}{b_e}\right)^2} \qquad (8)$$

The parameter b_e is an appropriate representative value of the spectral line half-width and is defined as invariant along the non-homogeneous optical path. The local half-width, b, is related to b_e through the parameter F, which is assumed independent of ν.

Integration of Eq. (5), with the use of Eq. (8), yields the mathematical expression for the Ladenburg-Reiche curve-of-growth, now generalized for a non-homogeneous path.

$$W = \int_{\bar{\nu}-\infty}^{\bar{\nu}+\infty} a_\nu \, d\nu$$

$$= 2\pi\, b_e\, y_L\, e^{-y_L} \left[I_0(y_L) + I_1(y_L) \right] \qquad (9)$$

The functions I_0 and I_1 are modified Bessel functions, and y_L, formulated below, is the curve-of-growth parameter:

$$y_L = \frac{1}{2\pi\, b_e} \int_0^L PSF \, d\ell \qquad (10)$$

Two limiting expressions for Eq. (9) that are widely used are the weak line approximation

$$y_L \to \infty \; ; \quad W \to \int_0^L PS \, d\ell \; ; \quad F \to 1 \qquad (11)$$

and the strong line approximation

Accurate, mathematically similar turbulent mixing layer profiles agreeing with classical solutions have been obtained.

Furthermore, results pertaining to turbulent mixing in general are summarized:

As expected, initial turbulence levels and recirculation zones significantly enhance mixing.

For low subsonic velocities, profiles of turbulent mixing between dissimilar gases, as indicated by present experiments, still obey the classical incompressible formulations.

Mixing rate increases with increasing density differences between streams for the examined flow configuration.

Rotational Relaxation of HF

The rotational relaxation of HF in the nonburning flow system has been examined in detail. Results are presented in this section, while the rotational behavior of the tracer in combusting flows is discussed in the next section. For a jet flow condition nearly identical to that described by Fig. 10 for the "near" position, i.e., HF seeded air mixing with air for T = 303°K and u = 45 meters/second at $z/r_0 = 2.5$, all observable HF R-branch spectral lines were monitored. The wavenumber scan shown in Fig. 2 was taken during this experiment. Radial distributions resulting from Abel inversion of the measured absorptances are presented in Fig. 15. The "off-center" peaks exhibited in these profiles for the lower valued spectral lines, particularly the R(0) line, result from apparent thermodynamic nonequilibrium of the HF and indicate rotational relaxation towards kinetic temperatures in the jet flow.

A plot of HF number density for individual states versus rotational quantum number is given in Fig. 16 for three radial flow positions. At the jet centerline (bottom plot) the solid straight line fit yields a rotational temperature of 420°K, e.g. see Eq. (19). This temperature is nearly equal to that of the "cracker" and HF piping system. Based on system errors and uncertainties in spectral line parameters, the most probable error limits have been determined and are indicated in Fig. 16, bottom plot. The resultant uncertainty in measured centerline rotational temperature is 360°K to 460°K. The dashed line in Fig. 16 indicates thermodynamic equilibrium at the jet centerline kinetic temperature of 303°K, plus expected number densities based on the upstream rotometer measurement of HF mass flow rate. Indeed, the HF appears to exhibit a rotational population distribution not in equilibrium with the kinetic temperature, plus an apparent loss in number density occurring between the rotometer and free jet system.

Possible corrections for HF spectral line half-widths and strengths have been calculated based on uncertainties in the measurements reported in Ref. 23 and 24. The corrections for line strength were found to be relatively small, while for line half-width, including uncertainties in foreign gas broadening effectiveness, corrections of -20% were determined to be possible. Accordingly, with these corrections, the HF number densities were re-evaluated; results are shown in the middle plot of Fig. 16. The rotation state appears to be populated according to $T_J = 405°K$ if the spurious behavior of the weak R(6) measurement is neglected.

Also shown in Fig. 16 (top plot) are the number density distributions measured at a radial position of $r/r_0 = 0.87$ and at the previously mentioned "off-center" peak obvious in Fig. 15. Examination of the top plot indicates increases in the ground state populations (R(0) line) compared to respective values based on rotational temperatures. A rotational population distribution differing from Maxwell-Boltzmann statistics with an apparent singular relaxation of the ground state towards the local kinetic temperature of 303°K is indicated.

Measurements of rotational temperature, determined via Eq. (19) using at least three separate spectral lines at a single field location, are summarized in Fig. 17 for all nonburning experiments. In Fig. 17, measured rotational temperatures are plotted versus HF partial pressure, as measured spectroscopically. Considerable scatter is noted in Fig. 17; nevertheless, lower values of HF partial pressure, usually implying flow expansion on the profile wings and at downstream locations, yields rotational temperatures nearly equal to the average jet kinetic temperature of 305°K. However, measurements (Experiments 4 and 7 for submerged single jets) at centerline locations near the nozzle exit for reduced relative HF flow rates and therefore reduced HF partial pressures show the same trend.

If the HF rotational relaxation in these experiments was a time dependent phenomena, one would expect most of the HF molecules to attain thermodynamic equilibrium in the "well-stirred" tank which exhibits a temperature of about 320°K and a mean residence time of 1 second, compared to the order of 1 millisecond residence time in the free jet system. (Also, it is interesting to note that for Experiment 7, a straight section of tubing, with a relatively small residence time, was substituted for the "well-stirred" tank.) Increased relaxation of the HF at low partial pressures indicates

13. Smith, D. F., "Infrared Spectra Analysis for Hydrogen Fluoride," Spectrochemica Acta, Vol. 12, 1958, p. 224.

14. Simmons, F. S., "Radiances and Equivalent Widths of Lorentz Lines for Nonisothermal Paths," J. Q. R. S. T., Vol. 7, 1967, p. 111.

15. Meredith, R. E. and Kent, N. F., "Line Strength Calculations for the 0 → 1, 0 → 2, 0 → 3, and 1-2 Vibration-Rotation Bands of Hydrogen Fluoride," Willow Run Laboratories, Report 4613-125-T, The University of Michigan, 1966.

16. Jarry, R. L. and Daves, W., Jr., "The Vapor Pressure Association, and Heat of Vaporization of Hydrogen Fluoride," J. Am. Chem. Soc., Vol. 57, 1953, p. 600.

17. Long, R. W., Hildebrand, J. H., and Morrell, W. E., "The Polymerization of Gaseous Hydrogen and Deuterium Fluorides," J. Am. Chem. Soc., Vol. 65, 1943, p. 182.

18. Tollmien, W., "Berecknung Turbulenter Austreitungsvorgange," ZAMM, Vol. 6, 1926, p. 1. (Also, NACA TM 1085, 1945.)

19. Görtler, H., "Berechnung von Aufgaben der freien Turbulunz auf Grund eines neven Nakerungsansatzes," ZAMM, Vol. 22, 1942, p. 244.

20. Abramovich, G. N., The Theory of Turbulent Jets, M. I. T. Press, Cambridge, Mass, 1963.

21. Cohen, L. S., "A New Kinematic Eddy Viscosity Model," United Aircraft Research Laboratories Report G211709-1, East Hartford, Conn., 1968.

22. Taylor, G. I., "The Transport of Vorticity and Heat Transfer Through Fluids in Turbulent Motion," Proc. Roy. Soc., London, Vol. 135A, 1932, p. 685.

23. Smith, D. F., "The Overlapping Hydrogen Fluoride Monomer Dimer Spectra," J. Molecular Spec., Vol. 3, 1959, p. 473.

24. Lovell, R. J. and Herget, W. F., "Lorentz Parameters and Vibration-Rotation Interaction Constants for the Fundamental Band of HF," J. O. S. A., Vol. 52, 1962, p. 1374.

25. Gaydon, A. G., The Spectroscopy of Flames, John Wiley and Sons, Inc., New York, 1957.

26. Oss, J. P., "Absorption and Emission Coefficient Determination by a Zonal Ring Technique in a Circular Plasma Column," Aerospace Research Laboratories Report ARL 66-0110, Wright Patterson Air Force Base, Ohio, 1966.

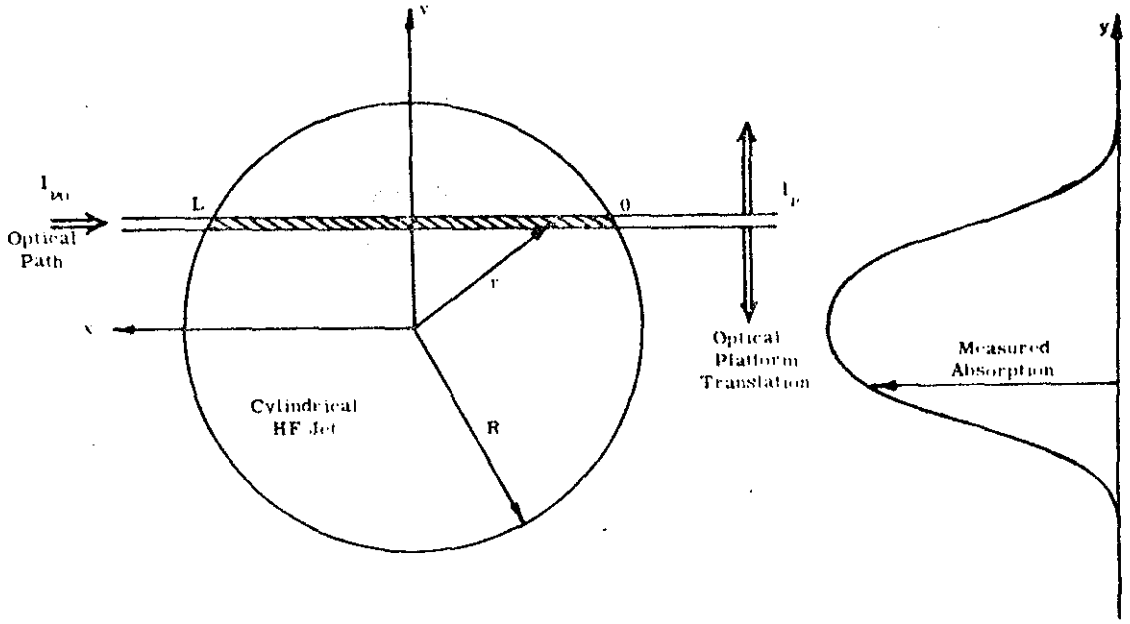

Figure 1. Schematic of Cylindrical Jet and Optical Path.

Approximate Experiment Conditions

HF Pressure:	0.03 atm
Air Pressure:	0.95 atm
Temperature:	300 °K
Path Length:	1 cm
Slit Width:	70μ

Figure 2. HF Absorption Spectrum Showing R-Branch of Fundamental Vibration-Rotation Band.

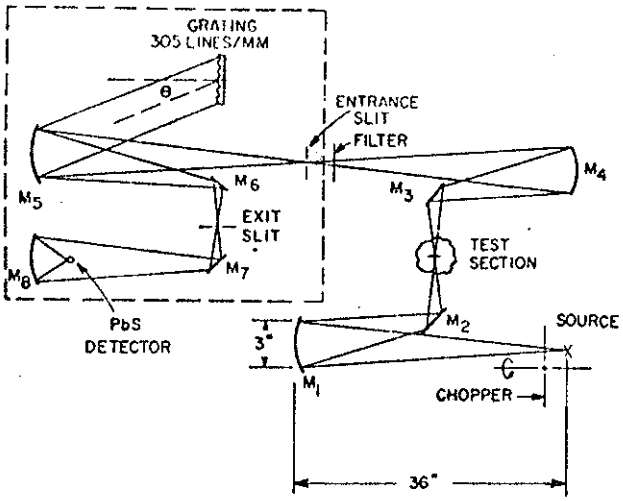

Figure 3. Monochromator and Entrance Optics Physical Schematic

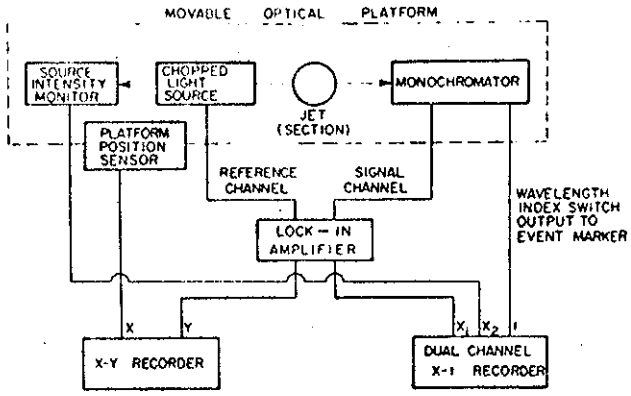

Figure 4. Block Diagram of Optical Instrumentation.

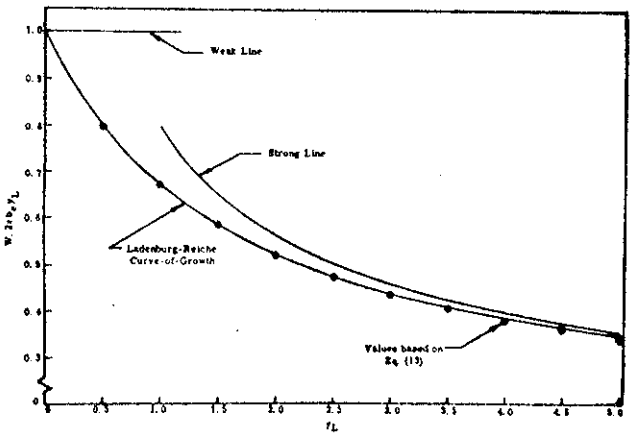

Figure 5. Equivalent Width for Lorentzian Absorption.

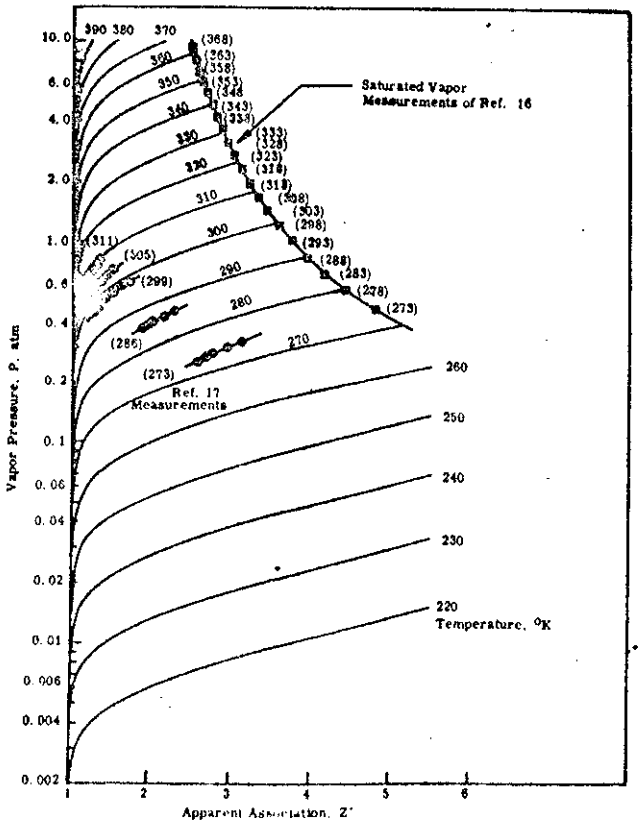

Figure 6. Apparent Association for Gaseous Hydrogen Fluoride.

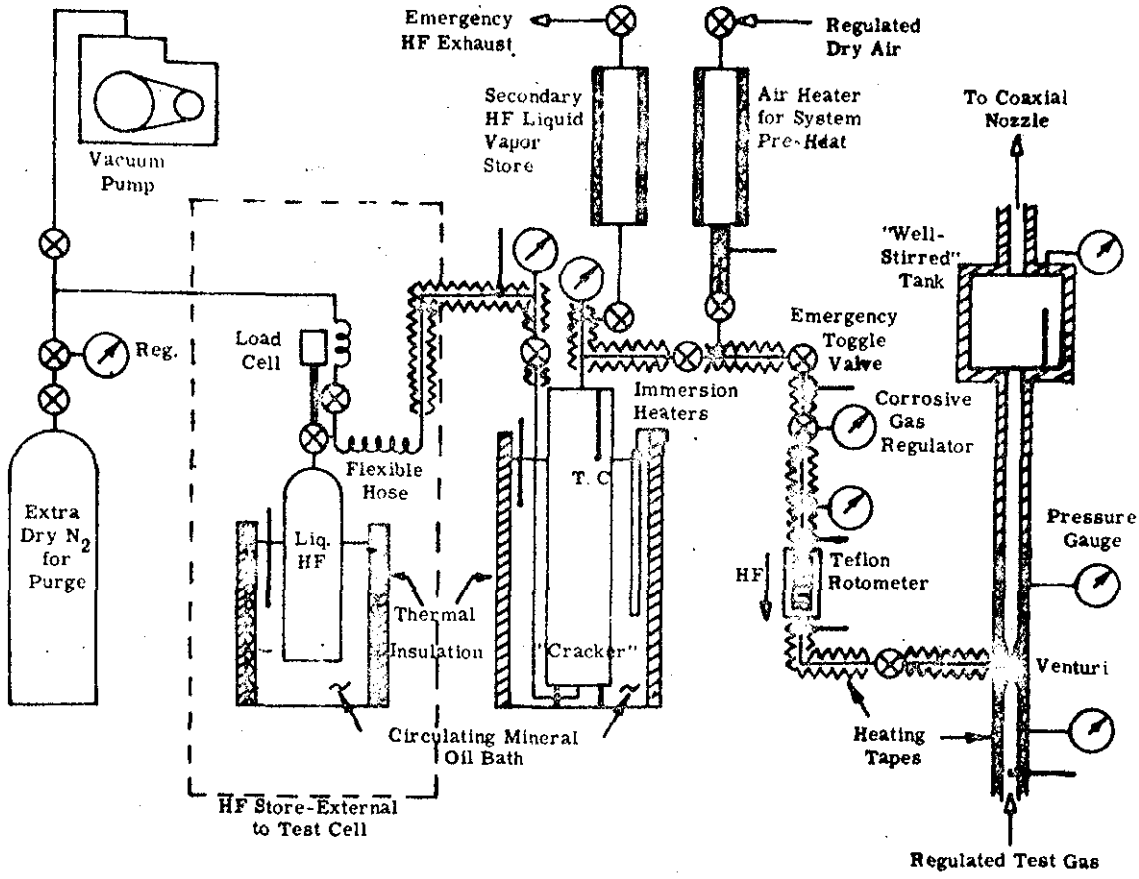

Figure 7. Schematic of Hydrogen Fluoride Delivery System.

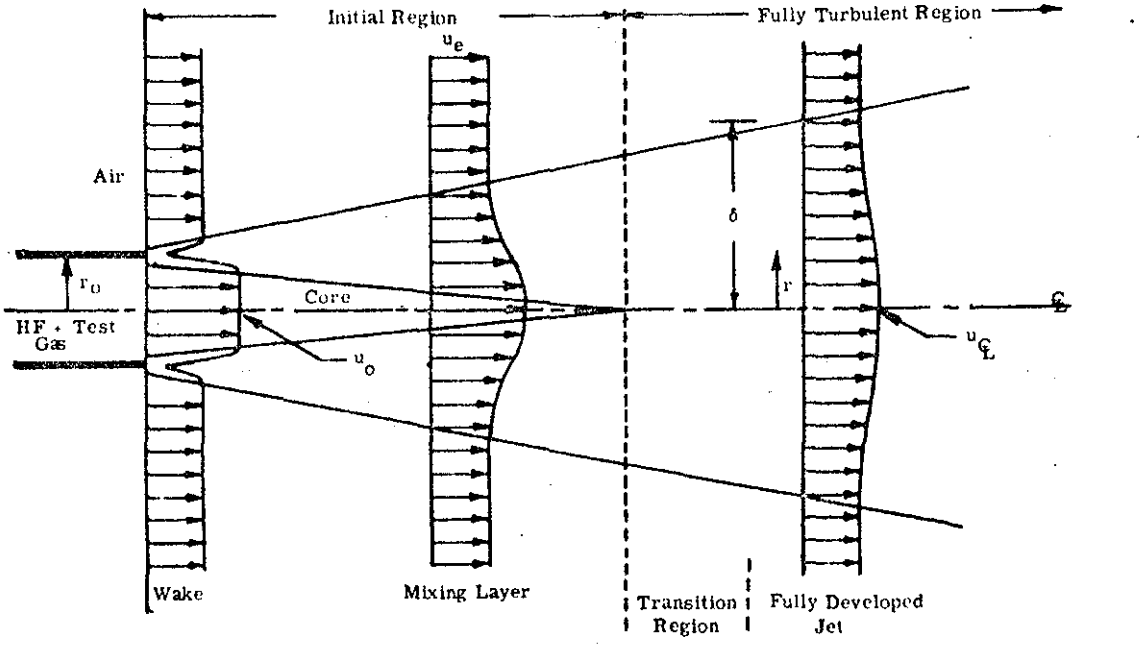

Figure 8. Turbulent Mixing of Coflowing Streams.

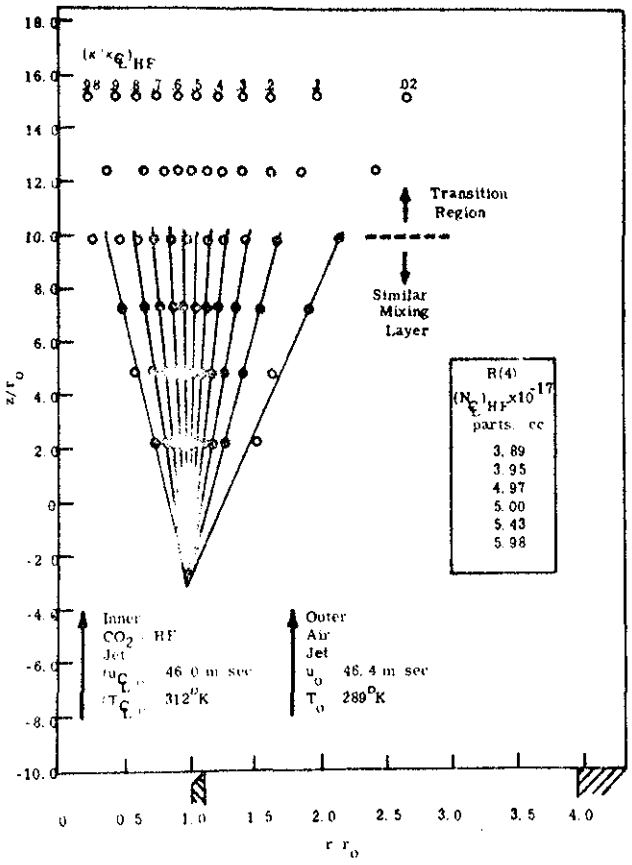

Figure 13. Tracer Spread in Coaxial Jet with Inner CO_2 Stream.

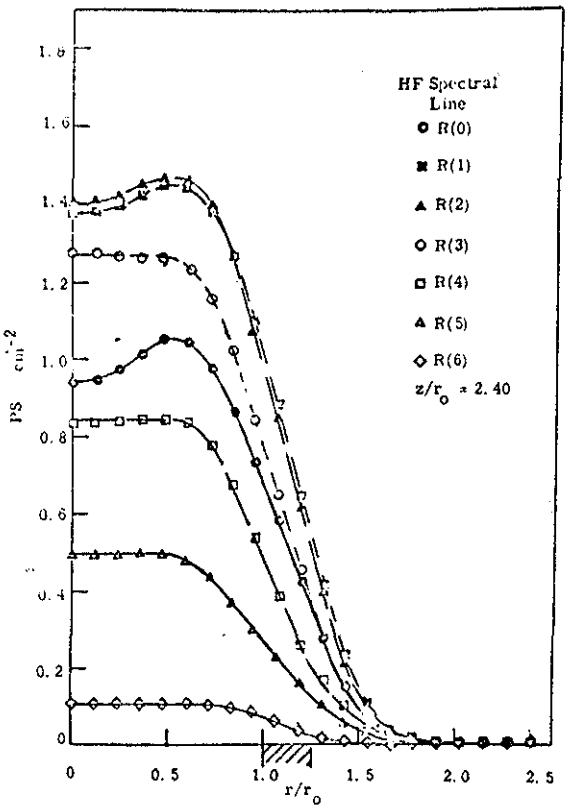

Figure 15. Experiment 1: Radial Distributions of PS for HF Obtained by Abel Inversion.

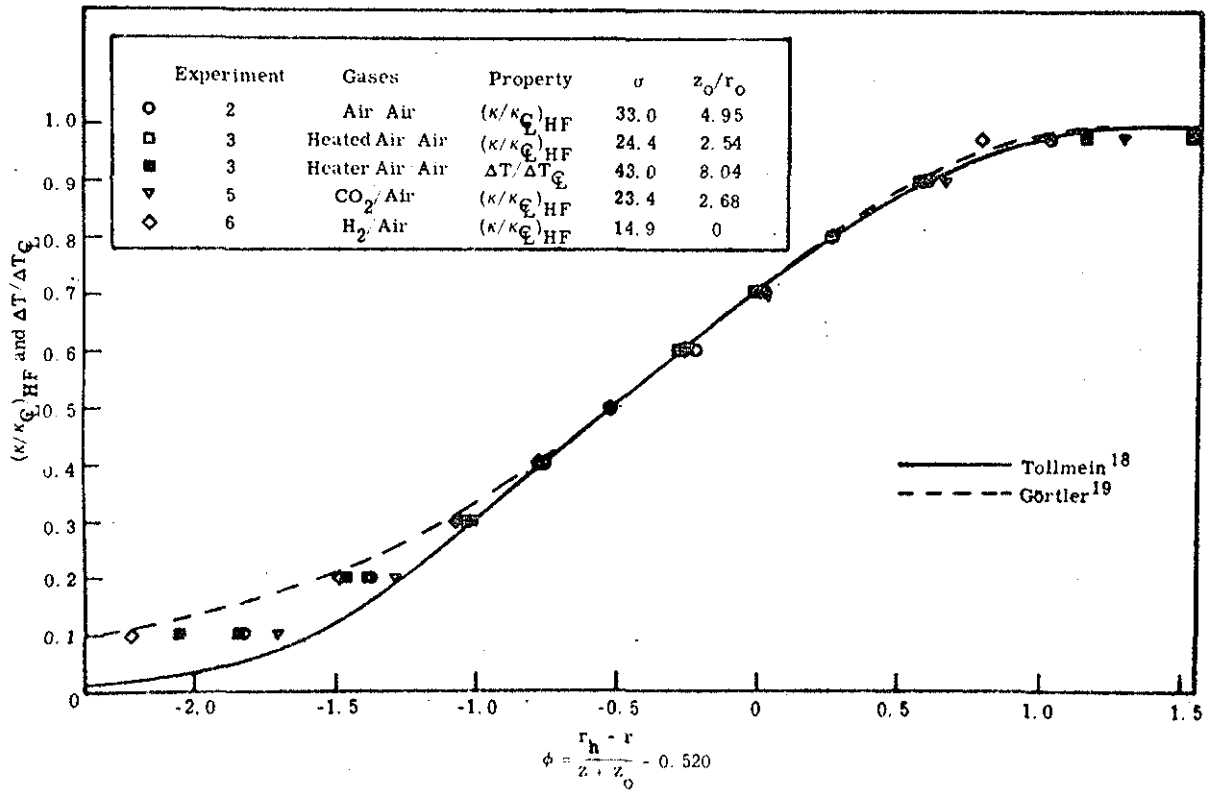

Figure 14. Mixing Layer Similarity Profiles for Concentration Admixture and Excess Temperature.

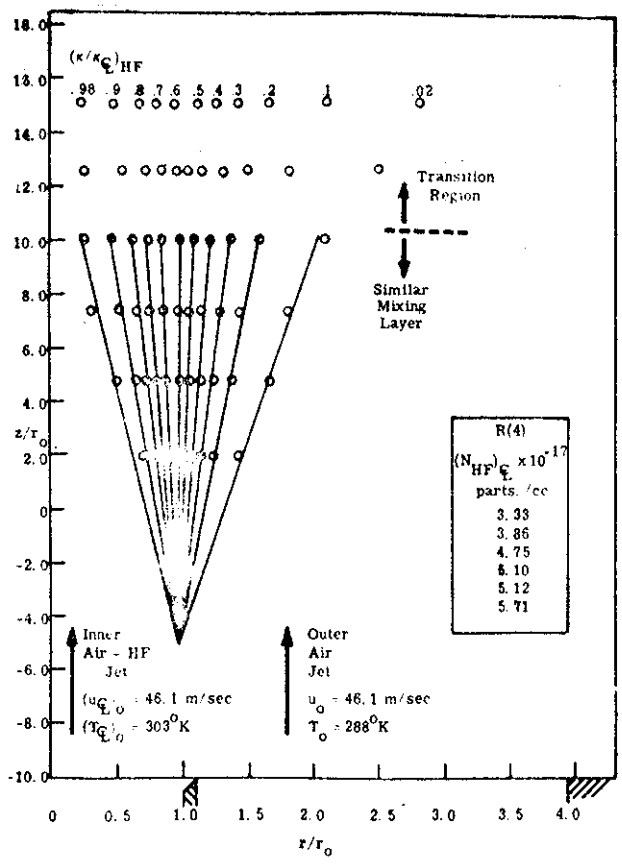

Figure 9. Tracer Spread in Coaxial Air Jet

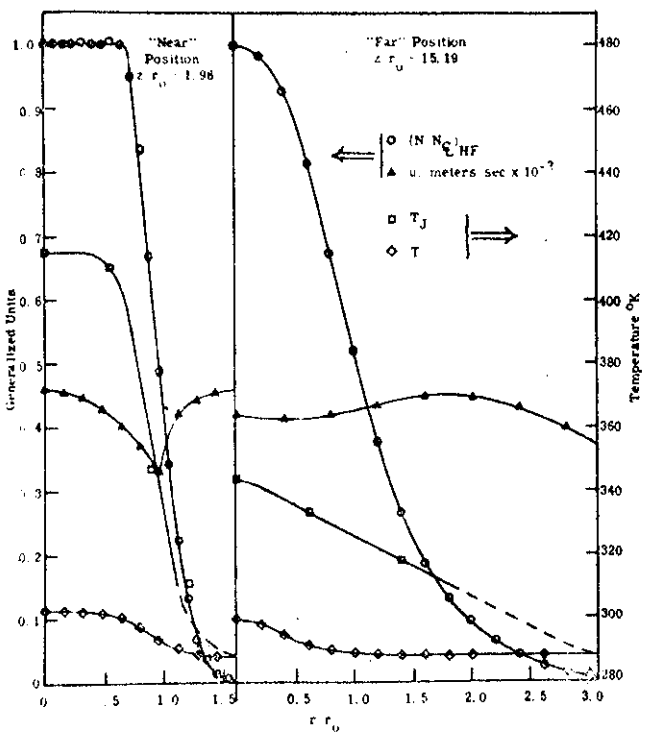

Figure 10. Experiment 2: Radial Distributions of Velocity, Kinetic Temperature, and HF Number Density and Rotational Temperature.

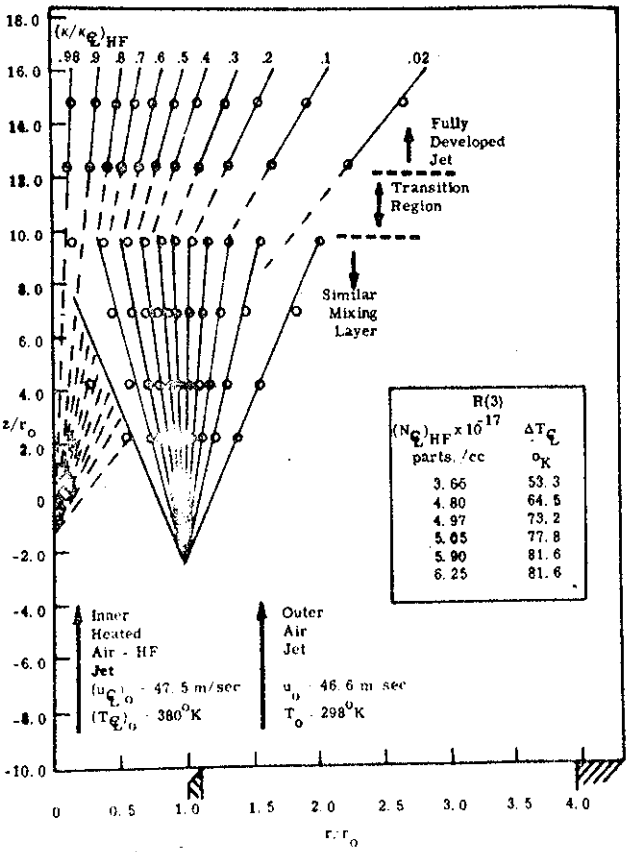

Figure 11. Tracer Spread in Coaxial Air Jet with Heated Inner Stream.

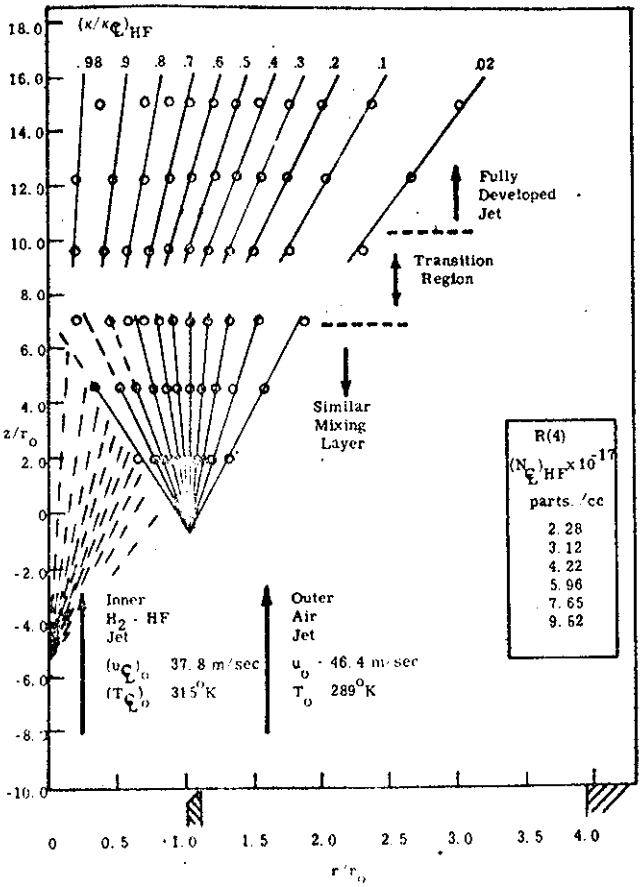

Figure 12. Tracer Spread in Coaxial Jet with Inner H_2 Stream.

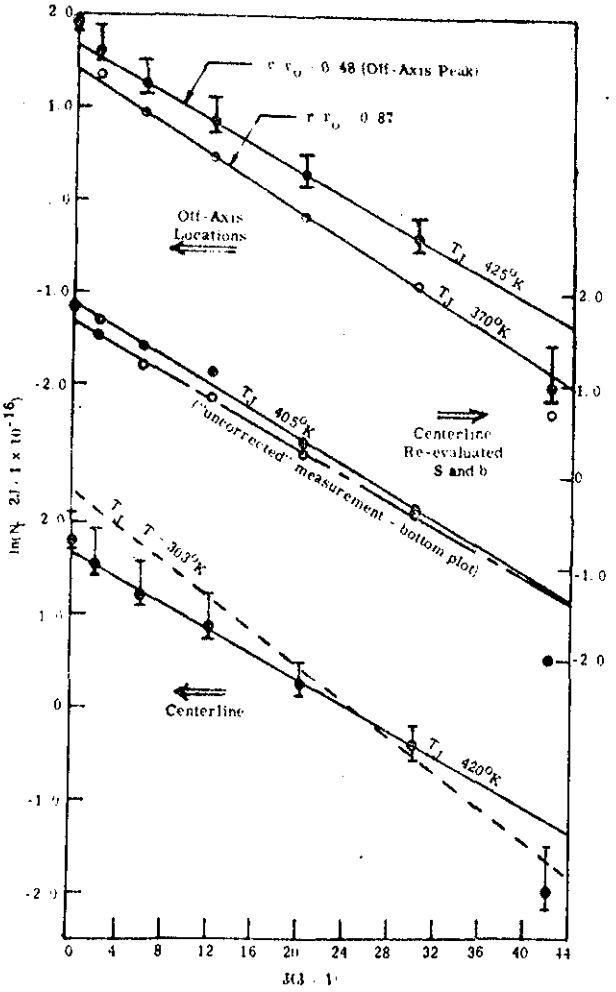

Figure 16. Experiment 1: Rotational Populations and Temperatures for HF.

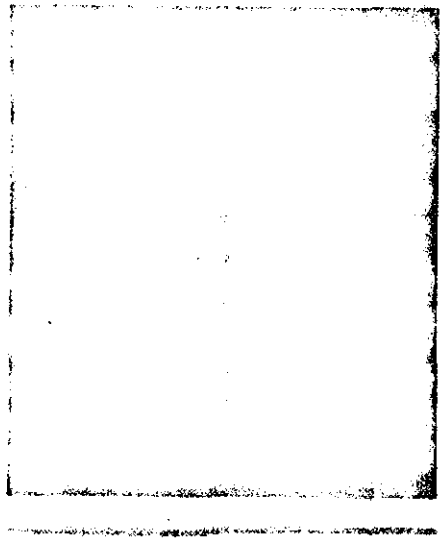

Figure 18. Schlieren Photograph of Reacting Coaxial Jet.

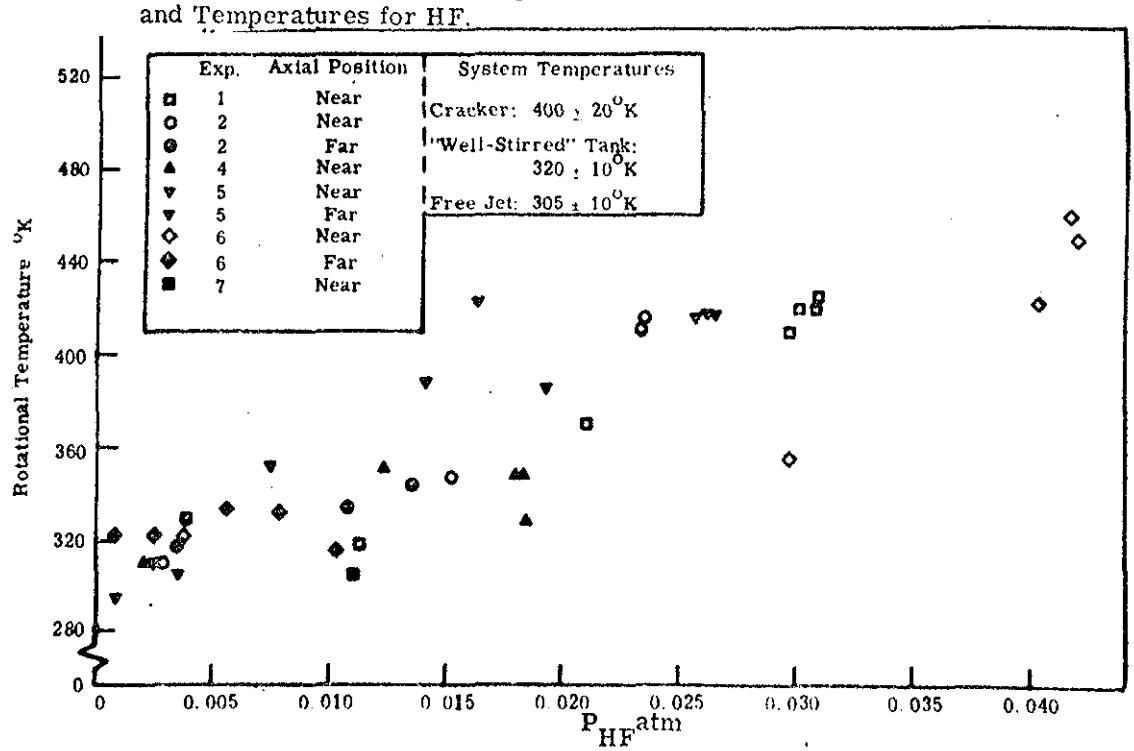

Figure 17. Variation in Turbulent Spread Parameter for Mixing Layers between Disimilar Streams at Nearly Equal Low Subsonic Velocities.

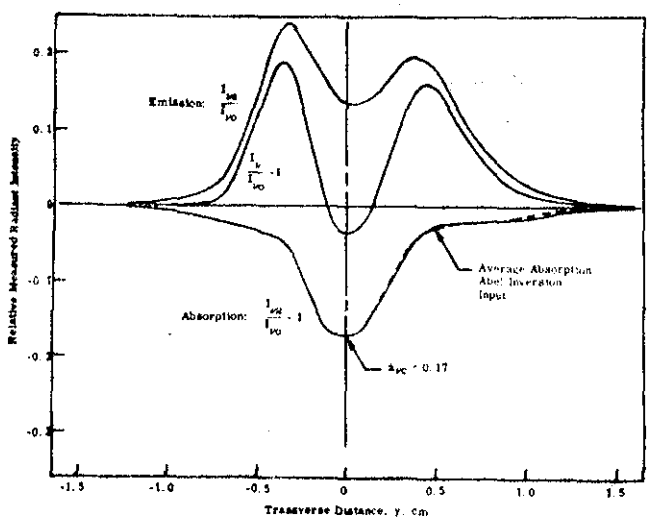

Figure 19. Measured Line Radiation in HC Flame for HF at R(3) and $z/r_o = 17.43$.

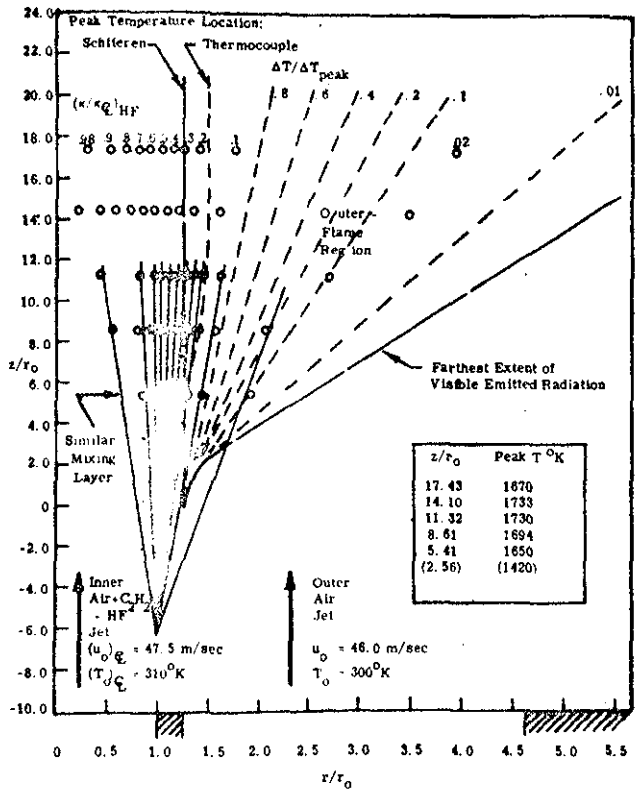

Figure 20. Turbulent Spread in Reacting (HC Flame) Coaxial Jet.

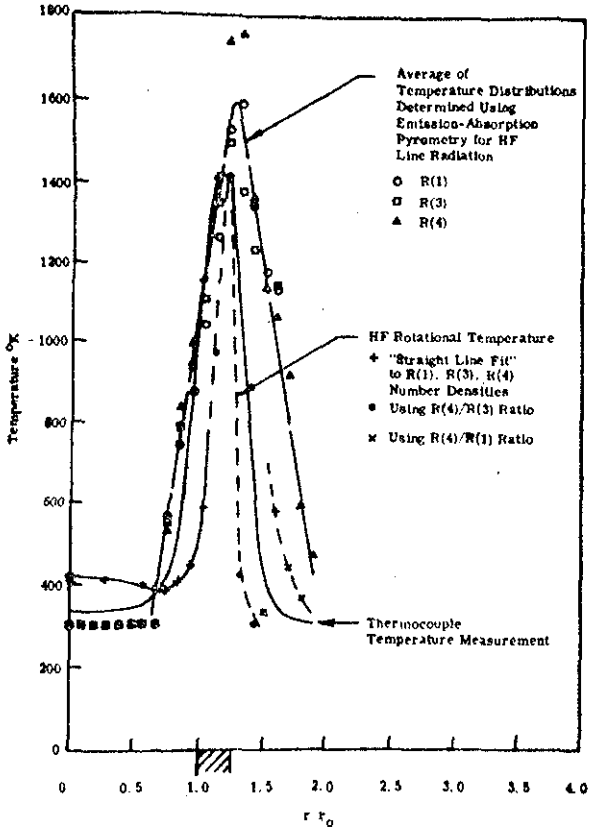

Figure 21. Kinetic and HF Rotational Temperature Measurements in HC Flame at $z/r_o = 2.56$.

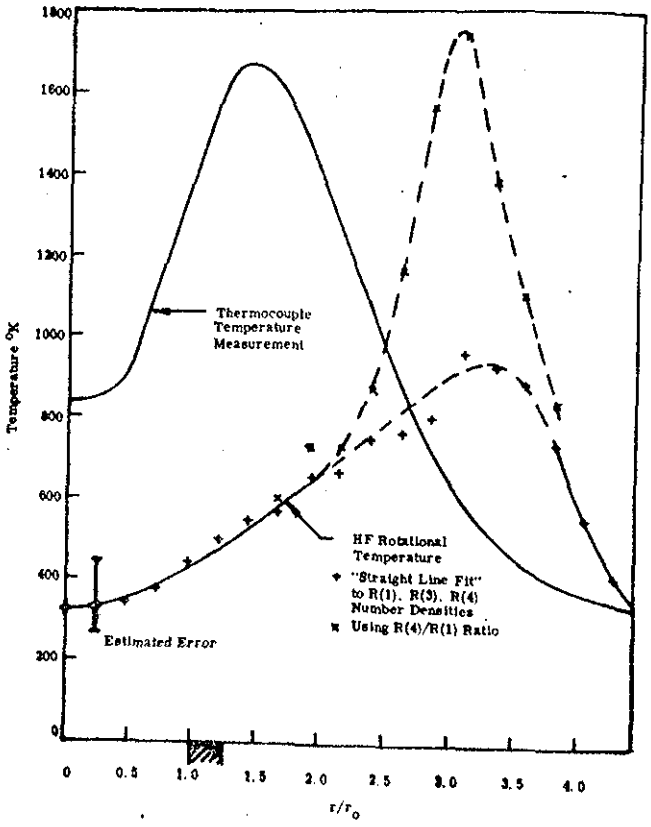

Figure 22. Kinetic and HF Rotational Temperature Measurements in HC Flame at $z/r_o = 17.43$.